ILASS-Americas 22nd Annual Conference on Liquid Atomization and Spray Systems, Cincinnati, OH, May 2010

A KIVA-based Model for Liquid Jet in Cross Flow

M. Behzad[1], A. Mashayek and N. Ashgriz
Multiphase Flow and Spray System Laboratory
University of Toronto, ON M5S3G8

Abstract

KIVA-III code was employed to model the atomization of a liquid Jet In Cross Flow (JICF). The liquid jet was represented by injecting single droplets into cross flow continuously and they were forced to follow the jet trajectory associated with an experimental correlation. Furthermore, these droplets were not allowed to go through aerodynamic breakup and collision. This takes account of wake region behind the jet, which might be important in secondary breakup of the droplets. In the present study, in order to model the droplet shedding along the liquid jet at high gas Weber number (i.e. shear breakup regime), a number of nozzles were located on both sides of the jet between the locations of the onset of the droplet shedding and the column breakup. The properties of theses nozzles including number, stripping mass rate, size and velocity of the droplets were obtained from phenomenological sub-models and experimental correlations. The results consisting of droplets size, velocity and volume flux distributions were compared with those of available experiments in a similar flow conditions. The model was able to capture the trend which existed in the experiments and there was a fare agreement between the droplets size and volume flux obtained by the model and the experimental results.

[1] Corresponding Author: m.behzad.jazi@utoronto.ca

Introduction

Liquid fuels are used in a wide range of combustion systems, such as in diesel engines, gas turbines, boilers, etc. In these systems, the liquid is atomized and sprayed into the combustor to increase the combustion efficiency and reduce emissions. With the recent interest in using alternative fuels, such as bio-fuel, and with the more stringent regulations on the emission levels, it is necessary to develop more improved combustor and fuel injector systems. More advanced and more accurate models are needed to simulate the fuel injection and combustion processes in order to reduce such development cost and time. The present article is aimed at developing one such model, namely, a model for the fuel injection in systems with cross flows, by means of a theoretical-numerical method. This type of fuel injection is common in gas turbine systems, since they provide a high rate of mixing.

Atomization of Liquid Jet in Cross Flow

Earlier experimental studies of the properties of non-turbulent liquid jets in cross-flows had been reviewed by Wu et al. [1] and Mazallon et al. [2]. They have been mainly focused on penetration height and jet/spray plume trajectories for various liquid jet and crossflow properties (Schetz and Paddye [3]; Nejad and Schetz [4]; Nygouan and Karagozian [2]; Wu et al. [1]).

Processes associated with the primary breakup of liquid jets in crossflows were investigated by Wu et al. [1], and they were extended by experimental studies of Mazallon et al. [2], Sallam et al. [6], and N.G et al. [7].

While liquid jet penetration, effects of liquid properties on jet breakup, and breakup processes have been studied extensively, few studies have measured the spray structure of an atomized liquid jet in the near- or far-field regions, particularly in elevated temperatures and pressures (Inamura and Nagai [8]; Wu et al. [1]; Becekr and Hassa [9]; and more recently Sallam et al. [6]; Lubarsky et al. [10]).

In a common modeling approach, the liquid column is represented as a set of discrete large drops with the same size of the real jet, rather than a coherent liquid jet issuing out of the nozzle and included with phenomenological sub-models for various features of jet disintegration. Furthermore, due to considerable similarities between single droplet breakup and the disintegration of a jet in crossflow [1,2], modeling of jet breakup mechanism has been mostly based on experimental correlations for individual droplets subjected to shock waves such as those presented by Chou et al. [11]. This type of modeling mainly have focused on the shear breakup mechanism, since it is the dominant breakup mode in combustion applications (Rachner et al. [12]; Madabhushi [13,14]; Khosla et al. [15]).

Following the above-mentioned modelings, the objective of the present article is to develop a new practical model for the atomization of liquid jets in crossflows in shear breakup regime (high gas Weber number) using several phenomenological sub-models and empirical correlations which are basically for jet breakup rather than individual drops.

These sub-models comprise of models for liquid jet trajectory, surface mass removal rate, location of injection points, and initial size and velocity of droplets produced in primary atomization. KIVA-III code was modified and utilized to capture the entire process of jet atomization.

Existing Sub-models for Jet Breakup Processes

In this section the available sub-models for different aspects of jet atomization will be discussed. They have been developed primarily for shear breakup regime due to its many applications.

There is a unanimous agreement in experimental studies that the jet trajectory is primarily a function of liquid-to-gas momentum flux ratio (q), nozzle diameter and downstream distance. However, some studies have included other parameters such as the gas Weber number (We_g). Since the main goal of the current study was the modeling of primary atomization of the liquid jet, we simply applied the well-known phenomenological model developed by Wu et al.[1], owing to its simplicity and universality acceptance among other correlations;

$$\frac{y}{d_j} = 1.37\sqrt{q\frac{x}{d_j}} \tag{1}$$

however it would be easy to apply a more complicated model for trajectory [16].

The study also considered the column fracture location, i.e. the gas-streamwise distance from the nozzle exit to column fracture point as follows;

$$\frac{x_b}{d_j} = 8.06 \tag{2}$$

The common model which has been employed in the proceeding literatures for droplet stripping from the liquid jet surface is the Boundary-Layer-Stripping (BLS) model introduced by Ranger and Nicholls [17]. The model was developed on the basis of experimental observations of drops exposed to shockwave. It considered the shear breakup phenomenon of drops as a result of a boundary layer stripping mechanism. The model has also been applied for droplet stripping from the periphery of jets based on the similarities of shear breakup of liquid jets and drops. However, some

modifications have been considered (Khosal et al. [15]; Mashayek et al. [16]; Delaplanqua [12]).

Recently, Sallam et al. [6] employed the pulsed holography technique to penetrate the dense spray region and observed the surface properties of liquid jet shear breakup. In the present study, their conceptual sub-models and correlations for different features of jet primary breakup were applied. In the following, a brief review of mentioned sub-models will be presented.

In their experiments, the mass flux of liquid drops leaving the liquid surface due to primary breakup along the liquid column was investigated. They observed that the drops formed by primary breakup only leave the liquid column over its downstream half. Thus, the liquid removal rate over this downstream projected area was averaged to find the mean mass flux, $\dot{m}_l''$, of drops leaving the liquid column with a gas-streamwise relative velocity, u_p specified later. Hence; a liquid surface breakup efficiency factor ε was defined as,

$$\varepsilon = \frac{\dot{m}_l''}{\rho_l u_p} \tag{3}$$

Then a correlation was fitted to the measurements of ε for non-turbulent round liquid jets in gaseous crossflow as follows;

$$\varepsilon = 6.89\times10^{-4}\exp(\frac{5.43y}{y_b}) \tag{4}$$

in which y_b is the jet-streamwise location of column breakdown point.

When a liquid jet is issued to a cross flow, two types of waves appear; column waves involving deflection of the entire column, and surface waves with smaller wavelengths. The surface waves become visible on the upstream side of jet at larger value of We_g, and they do not penetrate into the jet core. The wavelength of the surface waves decreases as the gas Weber number increases.

Several experimental observations have suggested that in shear breakup regime, the surface waves are associated with the distance between ligaments being stripped from the sides of liquid column. These waves initiate from the column periphery and extend to the leeward sides. Subsequently small droplets are stripped off from the end of these ligaments by the airstream [2,6]. This hypothesis was applied in the current modeling in order to estimate the stripping location along the jet. The following correlation was used for wavelength of surface waves [6];

$$\frac{\lambda_s}{d_j} = 3.40We_g^{-0.45} \tag{5}$$

Another feature of the primary breakup is the time of onset of breakup (taken at the condition where ligaments/drops just begin to form at the liquid surface). Sallam et al. postulated a mechanism for ligament forming similar to BLS model. They also assumed that the diameter of the ligament at onset should be the same order as the thickness of liquid shear layer. Based on these assumptions, the following correlation for the onset of ligament was derived,

$$\frac{t_i}{t_v^*} = 0.0004[\frac{(\mu_l/\mu_g)}{We_g}] \tag{6}$$

and the location of the onset of ligament formation can be calculated approximately as follows,

$$y_i = v_j t_i \tag{7}$$

Furthermore, the variation of ligament sizes along the surface was assumed to involve a transient regime in which the thickness of shear layer (and consequently ligament diameter) at the separation point is growing as a function of time, and a quasi-steady regime where the thickness becomes a fixed fraction of liquid jet diameter, which in turn is taken to be proportional to initial liquid jet diameter. By verifying these assumptions through experiments, the following relations were suggested for transient and quasi-steady regime respectively [6];

$$\begin{aligned} d_{lig}/d_j &= 3.6[\nu_l y/(v_j d_j^2)]^{0.5} \quad \nu_l y/(v_j d_j^2) < 0.001 \\ d_{lig}/d_j &= 0.11 \qquad\qquad\qquad\quad \nu_l y/(v_j d_j^2) > 0.001 \end{aligned} \tag{8}$$

Finally, assuming a Rayleigh breakup mechanism, the droplets diameter was obtained;

$$d_p = 1.2 d_{lig} \tag{9}$$

In the last step towards the surface properties investigation in Sallam et al.'s study, droplet velocities were examined. The measurements were close to the tips of ligaments to minimize the effects of drop velocity relaxation to the ambient velocity. The resulting velocity correlations of the measurements are as follows;

$$\begin{aligned} v_p/v_j &= 0.7 \\ u_p(\rho_l/\rho_g)^{0.5}/u_\infty &= 6.7 \end{aligned} \tag{10}$$

It is evident that both components of the droplet velocity are independent of the drop diameter.

Numerical Implementation

In this section the procedure of assembling previously explained sub-models and correlations to build a conceptual-numerical model for the jet in crossflow atomization will be presented. In order to be able to implement the sub-models in the code, several modifications must be done on the source code. The modeling steps are illustrated in Fig. 1.

We start from the modeling of the jet itself. Since the code can only deal with the liquid phase in droplet form, for modeling the jet, individual droplets (hereafter called jet-droplets) are injected from the jet injector. Although, it is obvious that a liquid jet is inherently different from the individual droplets, the jet induced aerodynamic effects can be relatively reconstructed by injecting droplets. The injection mass rate and droplet sizes are determined based on the real initial jet diameter and flow rate. Then the jet-droplets are forced to follow appropriate jet trajectory obtained by Eq. (1) until they reach the column fracture point, calculated by Eq. (2), where they are destroyed and ignored from spray domain of the problem. In addition, the jet-droplets remain intact by not being considered in the breakup, collision and evaporation subroutines of the code; although they are allowed to be distorted until column fracture point. This can be done by dividing the whole droplets of the domain into two types; the jet-droplets and stripping-droplets. Thus in this case, the stripping-droplets are real droplets subjected to different processes such as breakup and collision, but the jet-droplets are prohibited from those. In order to have two types of droplets, adjustments in subroutines associated with Lagrangian phase of the computation are required.

To model the shear breakup, several injectors are located along the jet. These injectors are described based on the properties of the shedding droplets as explained in the preceding section, and these are consisting of the location, mass rate, size and velocity of the stripping-droplets along the jet trajectory. In addition, in order to resemble real droplet shedding from sides of the jet, two nozzles at each transverse height are located from the onset of ligament formation (Eq. 7) to the column breakdown point (Eq. 2), and therefore the total number of injectors is multiplied by two.

As it was previously mentioned, in shear breakup regime the surface waves on the upstream side of the jet are likely responsible for producing ligaments which consequently break up to the droplets by a Rayleigh-like breakup mechanism [1,2]. Thus, we assume that the vertical distance between the spray injectors location along the column corresponding to stripping-droplets (i.e. L) is equal to the wavelength of surface waves (λ_s) estimated by Eq. (5). With this assumption, the required number of stripping injectors and their location along the jet trajectory can be calculated.

The mass flux of the stripping injectors is approximated by taking integration of Eq. (4) over the distance between each two nozzles (one wavelength) and then using Eq. (3). Hence, the mass rate of every two nozzles at each transverse location (y) can be calculated by multiplying the calculated mass flux by projected area, i.e. $d_j \times L$. This mass rate is divided by two to allocate the contribution of each nozzle.

The size of droplets for each nozzle is calculated by applying Eqs. (8) and (9) considering both transient and quasi-steady regimes for boundary layer formation. It should be mentioned that in order to have a more realistic droplet generation at the injectors, it is assumed that the calculated droplet size is Sauter Mean Diameter (SMD) and therefore the code can produce a droplet distribution for size based on a χ^2-distribution. Finally the velocity of the stripping-droplets at the nozzles would be calculated by Eq. (10).

By calculating the total mass rate of droplet stripping from the entire column and subtracting this amount from the initial jet flow rate, the mass rate associated with column fracture can be estimated. Subsequently, a nozzle is considered for the droplets produced as a result of column disintegration. Due to the lack of understanding of dynamics of the liquid column disintegration as a whole in shear breakup mechanism, it is inevitable to make crude assumptions for the size and velocity of produced fragments. Thus, in this study it is postulated that the velocity of droplets produced as the result of column fracture is the same as the initial jet velocity with the same direction, and the frequency of droplet generation (number of droplets injected per second) in column breakdown point is equal to the frequency of jet-droplets injected at the primary nozzle. The latter assumption can then be applied towards approximation of the size of the droplets generated from column fracture, which is of the same order of jet initial diameter. It is worth mentioning that based on the Eqs. (3) and (4), the total mass stripped from the downstream side of the jet is approximately 95% of total injected mass. Fig. 2 shows a schematic of modeling setup with the spray injectors located along the jet.

Results

In this section, the results of a jet in crossflow modeling are presented. The test case is similar to one of the experimental tests conducted by Wu et al. [18] for non-turbulent water jet injected into air crossflow at normal temperature and pressure. The spray structure in terms of droplets size, velocity and volume flux were calculated in the centerline of spray plume at x/d_j = 200. The nozzle diameter was 0.5 mm from which a water jet is injected into a Mach 0.3 air crossflow (i.e.

u_∞ = 103) with initial velocity of 19.3. These test conditions resulted in gas Weber number of 123 and momentum flux ratio of q = 21.7.

The computational domain (Fig. 3) consisted of a duct with a width and height of 75 mm and a length of 170 mm, various spray injectors, solid walls and inflow-outflow boundary conditions. The duct was composed of six blocks with different grid resolution. The lower-central block, with dimension $70d_j$ and $50d_j$ in y and x direction respectively, had higher resolutions. Further refinement of mesh within this block did not alter the results. Its dimensions were based on the measured spray penetration and width of experimental results. The value of inflow specific turbulent kinetic energy was set to a typical value of 10% of gas specific kinetic energy and its turbulence length scale was set to 0.01 m.

The flow-filed reached a quasi-steady state condition after around 0.03 s. Thus, the mean spray characteristics at the centerline were computed after this time at increments of 2.5 mm in the transverse and spanwise direction which was the same as probe volume of PDPA used in experimental measurements. The averaging duration continued for 0.1 s. Increasing in the averaging time did not change the results.

Figures 4a and 4b shows the side-view and front-view of a water jet injected into air crossflow. The gas velocity in crossflow direction (x), jet-streamwise direction (y) and spanwise direction (z) are presented in Figs. 5a-5c. The effects of the jet and spray plume on the gas flow-filed and vortical structures can be observed in these figures. However, it is clear that the effects of the jet blockage on the gas flow are not significant.

The centerline properties of the spray are plotted in Figs. 6a-6c as a function of y/d_j. There is a gradual increase in the droplet SMD in the y direction. This is because the larger droplets can penetrate more into the crossflow due to their higher transverse momentum compared to the small droplets. Since the droplets produced from the column breakdown point are large, they lead to a high SMD at the upper boundary of the spray plume. In addition, Fig. 6a shows that the spray penetration is less than experimental measurements, since no droplets pass the probe volume at $y/d_j > 55$.

Figure 6b shows that the volume flux decreases from the center to the edges of the plume. The region of large volume flux corresponds to the spray core and indicates an area of high droplets density which contains a significant amount of injected liquid. The reason for discrepancy between the maximum volume-fluxes can be explained by inspecting the spray width shown in Fig. 4b. The spray width of the model is approximately $20d_j$ which is less than experimental value of ~ $50d_j$. This results in an increase in the maximum volume flux. The other possible reason might be the underprediction of the spray penetration, which leads to a decrease in the upper boundary volume flux, and hence an increase in the maximum flux. Nevertheless, the trend of the volume flux was captured quit well.

The velocity plot depicted in Fig. 6c, shows a wake region in both the experimental and the model results. The wake region produced by the model is shifted towards the upper spray boundary at $y/d_j \sim 45$ compared to $y/d_j \sim 20$ for the experiment. Wu et al. [18] pointed out that this wake region is caused by the presence of the liquid column and the momentum exchange between the liquid column wave and the airstream. However, comparing the droplet velocity profile with the volume flux in the present model shows that the wake is corresponding to the spray core region where the gas flow experiences a reduction in velocity owing to the effects of the spray plume and the cumulative momentum exchange between droplets and cross flow. This fact can also be inferred by changing the initial vertical velocity of the droplets (v_p) which causes the wake region to move along the jet. In other words, changing the initial velocity of the droplets in the y direction can alter the droplets momentum in the vertical direction, and consequently the location of the spray core region will be changed. Therefore, the initial value of the droplets velocity plays an important role in the spray trajectory and the velocity profile at the downstream. Furthermore, the lack of sufficient momentum exchange between the liquid jet column and the gas might be another reason for the difference between the location of the wake region in the experiments and the model; even thought the jet-droplets are being employed to reproduce the gas drag effects (Fig. 7).

Conclusion

In this study, several conceptual sub-models and experimental correlations were incorporated into KIVA-III code in order to simulate the jet in cross flow atomization for the high gas Weber number. The sub-models were developed based on the assumption of formation of a boundary layer inside the liquid jet calibrated with the experimental results. They were applied for modeling the primary shear breakup of a jet by considering the droplets shedding rate, and the initial size and the velocity of droplets stripped off along the jet. The spray properties at the far-field including the droplets size, velocity and volume flux were averaged and compared with the experimental results. The droplets size and the volume flux were in good agreement with the experiments; however, there was a discrepancy between the predicted velocity profile of the droplets and that of experiment particularly for the location of the wake region. The predicted wake region is far from the jet nozzle, as opposed to the

experiments. The major issues involve in the present model are as follows;
(1) underpridiction of the spray width and the penetration due to the insufficient dispersion of droplets in both the jet-streamwise and spanwise direction. This issue led to an increase in maximum volume flux.
(2) Absence of velocity variation of stripping droplets stripped off the jet that along with the first issue can cause the wake region dislocation.

Further investigations are being conducted to alleviate these issues.

Nomenclature

d jet diameter
q momentum flux ratio, $\rho_l v_j^2 / \rho_g u_\infty^2$
t time
t^* characteristic break up time, $d(\rho_l/\rho_g)^{0.5} / u_\infty$
t_v^* characteristic viscous time, d^2/ν_l
u gas-streamwise velocity
v jet-streamwise velocity
x gas-streamwise distance
y jet-streamwise distance
We Weber number, $\rho_g u_\infty^2 d/\sigma$
μ dynamic viscosity
ν kinematic viscosity
ρ density
σ surface tension

Subscripts
b location of breakup of entire liquid jet
g gas property
i location of onset of breakup
j initial jet property at injector
l liquid property
lig ligament property
p droplet property
∞ ambient gas property

References

1. Wu P, Kirkendall K, Fuller R, Nejad A. J Propul Power, 13(1):64-73, 1997.

2. Mazallon J, Dai Z, Faeth GM. Atomization and Sprays, 9(3):291-311, 1999.

3. Schetz JA, Padhye A. AIAA Journal, 15(10):1385-90, 1977.

4. Nejad AS, Schetz JA. AIAA Journal, 22(4):458-9, 1984.

5. Nguyen TT, Karagozian AR. J Propul Power, 8(1):21-9, 1992.

6. Sallam KA, Aalburg C, Faeth GM. AIAA Journal, 2(12):2529-40, 2004.

7. Ng CL, Sankarakrishnan R, Sallam KA. Int J Multiphase Flow, 34(3):241-59, 2008.

8. Inamura T, Nagai N. J Propul Power, 13(2):250-6, 1997.

9. Becker J, Hassa C. Atomization and Sprays, 12(1-3):49-67, 2002.

10. Lubarsky E, Reichel JR, Zinn BT, McAmis R. Journal of Engineering for Gas Turbines and Power, 132(2):021501 (9 pp.), 2010.

11. Chou W, Hsiang L, Faeth GM. Int J Multiphase Flow, 23(4):651-69, 1997.

12. Rachner M, Becker J, Hassa C, Doerr T. Aerospace Science and Technology, 6:495-506, 2002.

13. Madabhushi R. Atomization and Sprays, 13:413-424, 2003.

14. Madabhushi R, Leong MY., Hautman D.J. ASME turbo expo 2004, 1:697-704, 2004.

15. Khosla S, Crocker D.S. ASME turbo expo 2004, American Society of Mechanical Engineers, 1:797-806, 2004.

16. Mashayek A, Jafari A, Ashgriz N. AIAA Journal, 46(11):2674, 2008.

17. Ranger AA, Nicholls JA. AIAA Journal, 7(2):285-90, 1969.

18. Wu P, Kirkendall KA, Fuller RP, Nejad AS. J Propul Power, 14(2):173-82, 1998.

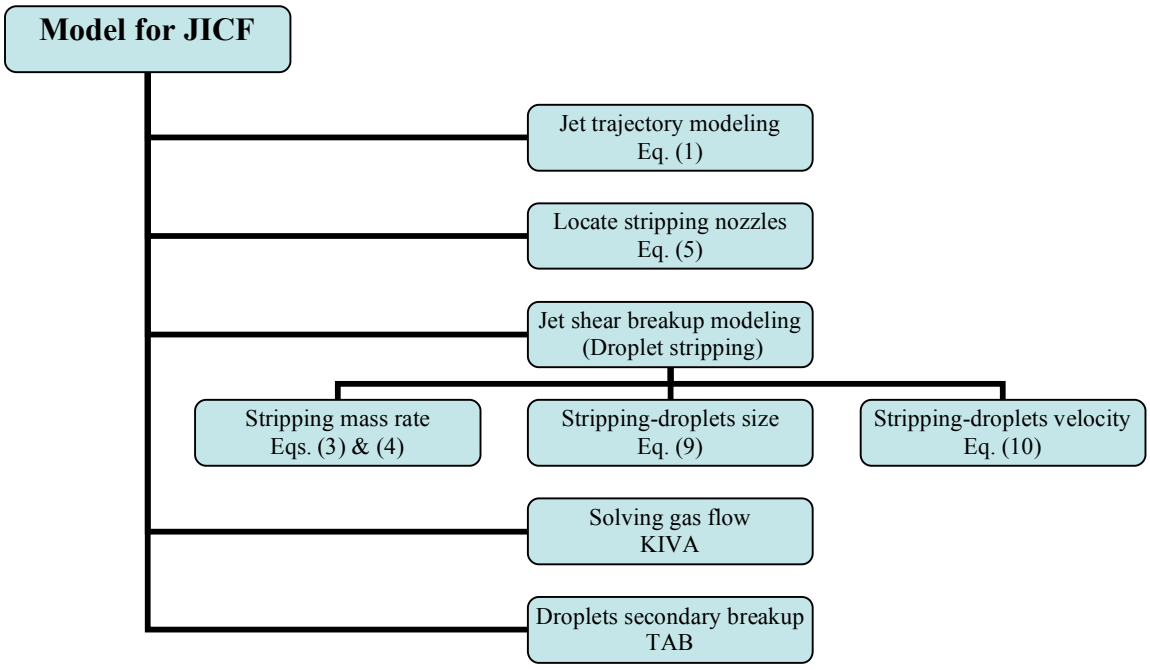

Figure 1. Jet in crossflow modeling procedure.

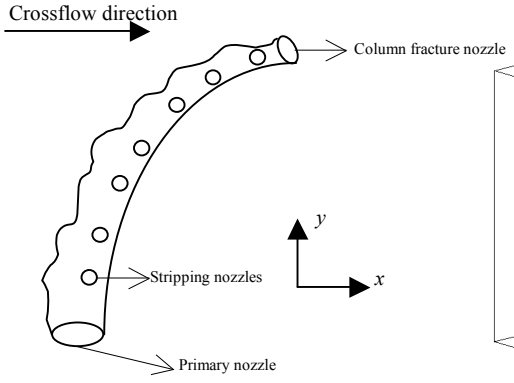

Figure 2. Schematic of a jet in crossflow modeling.

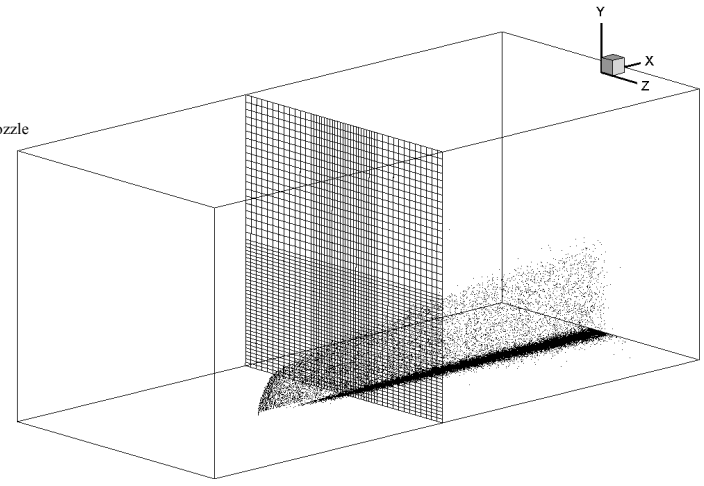

Figure 3. Computational domain.

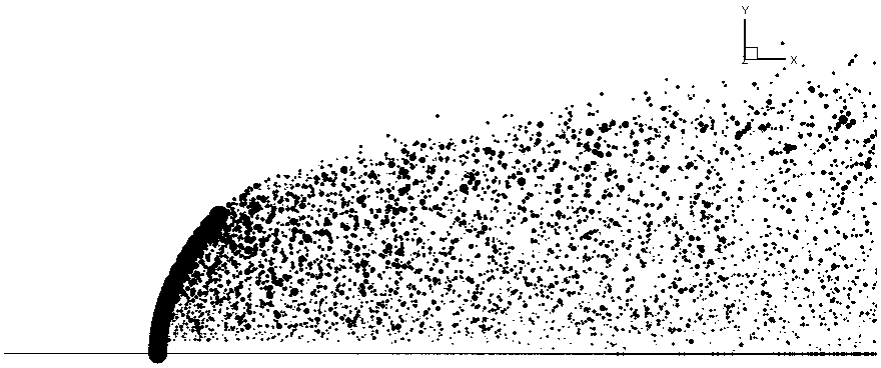

Figure 4a. Side-view of a jet in crossflow.

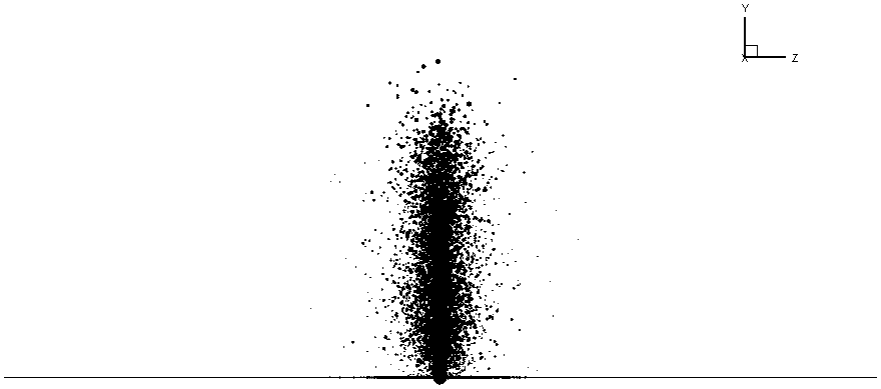

Figure 4b. Front-view of a jet in crossflow.

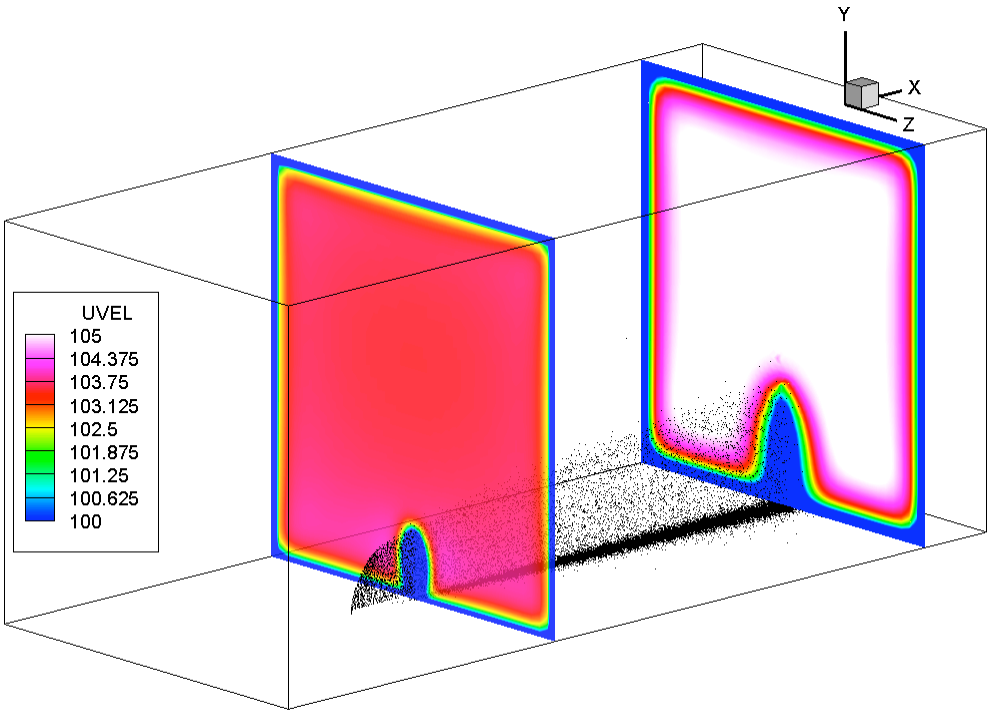

Figure 5a. Gas velocity (m/s) in crossflow direction.

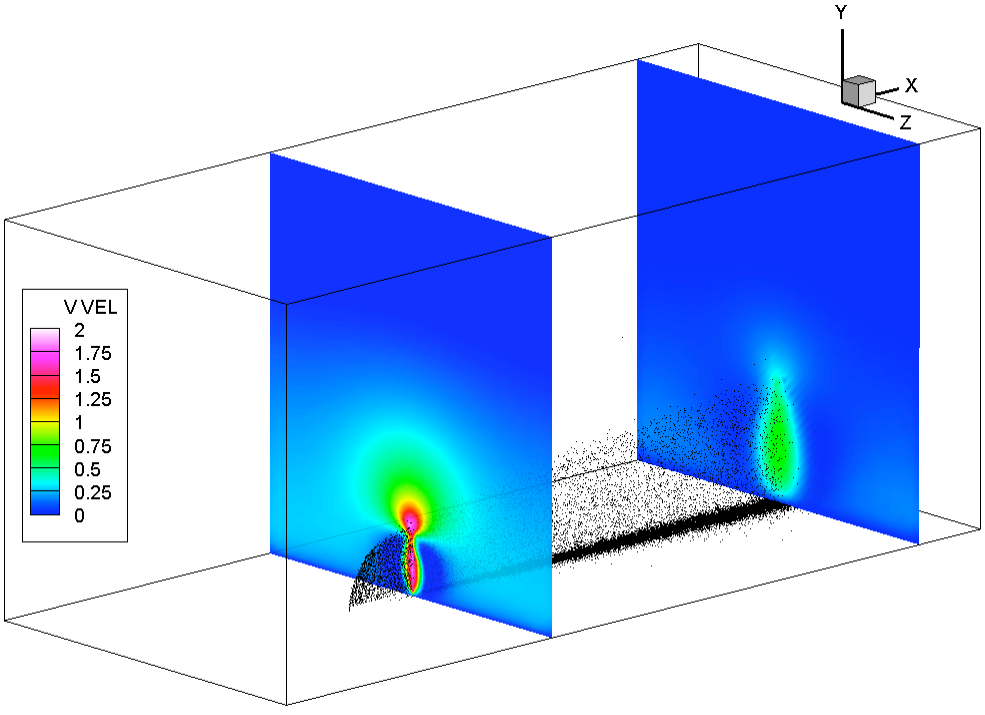

Figure 5b. Gas velocity (m/s) in jet-streamwise direction.

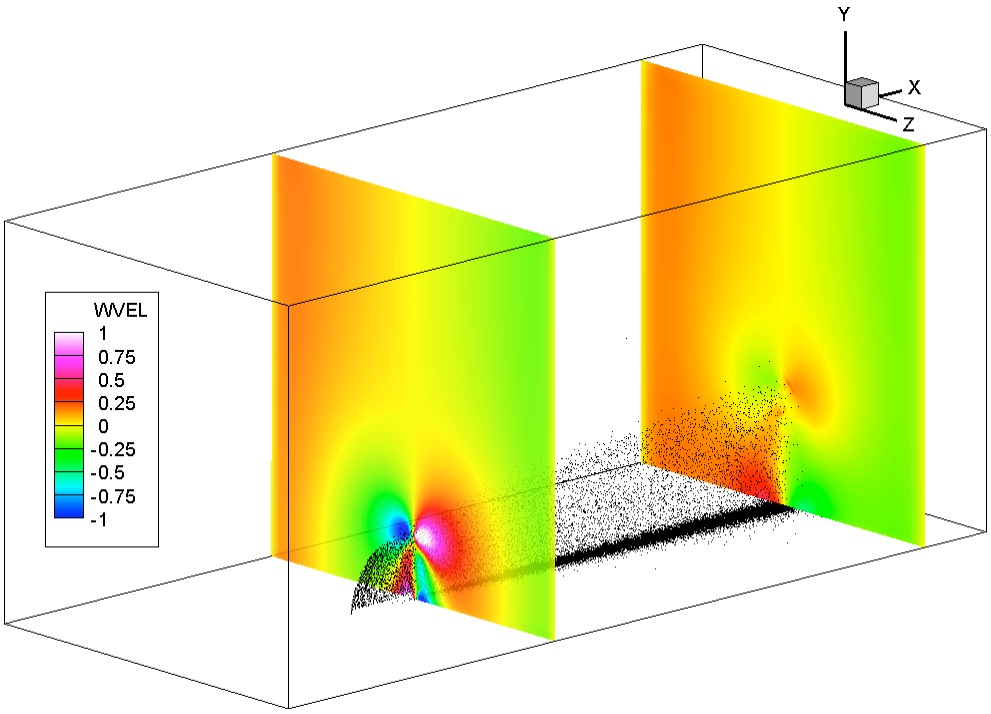

Figure 5c. Gas velocity (m/s) in spanwise direction.

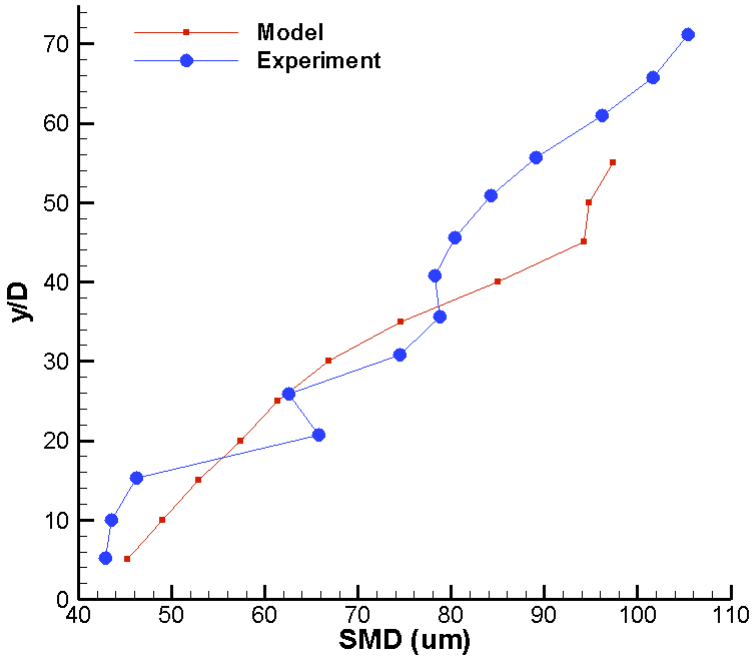

Figure 6a. Droplet size at 200*d*.

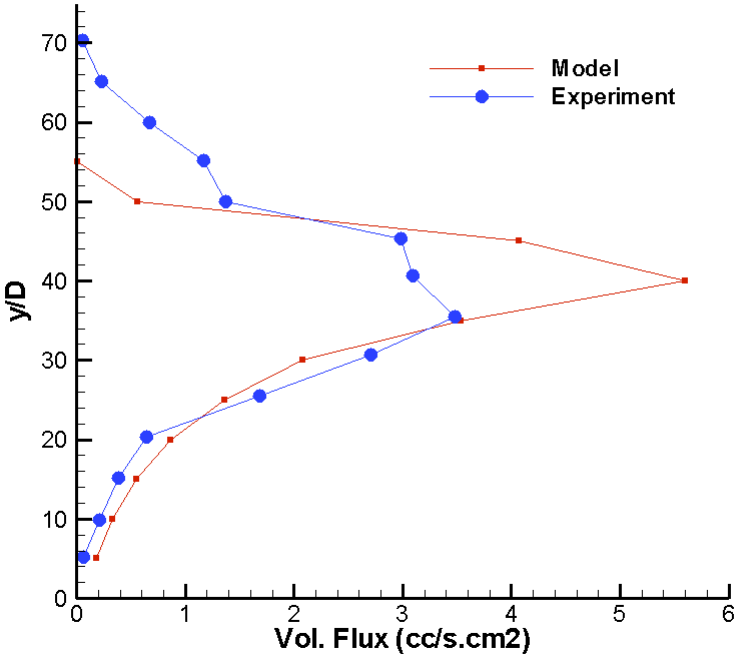

Figure 6b. Droplet volume flux at 200*d*.

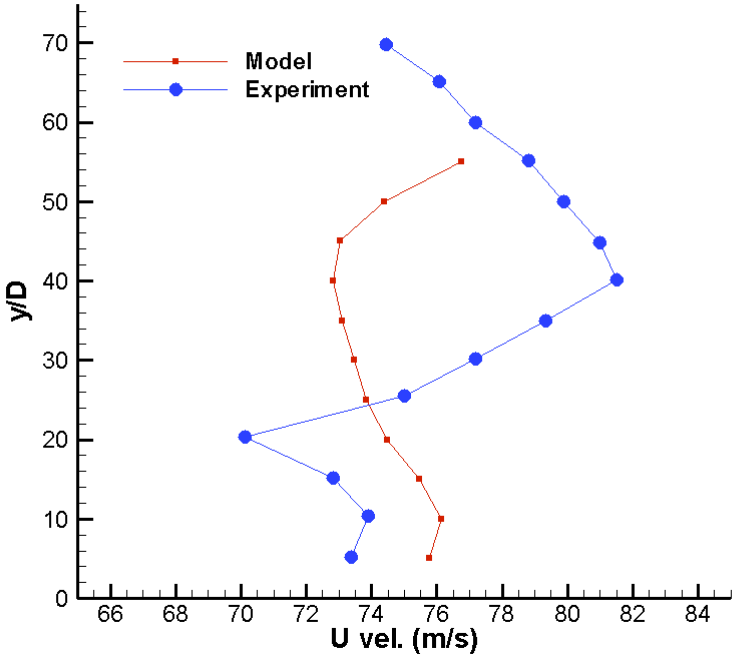

Figure 6c. Droplet velocity at 200*d*.

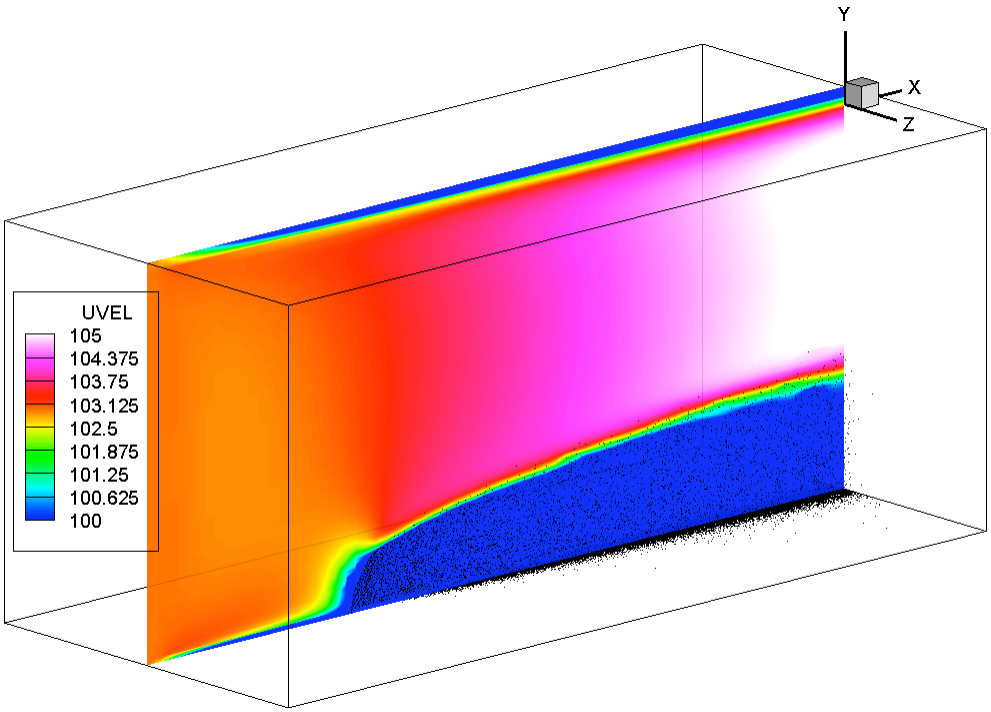

Figure 7. Effects of spray and jet on the gas velocity (m/s) in crossflow direction.